MATERIALS SCIENCE

# Smart covalent organic networks (CONs) with "on-off-on" light-switchable pores for molecular separation

**Jiangtao Liu[1], Shaofei Wang[1]*, Tiefan Huang[1], Priyanka Manchanda[1], Edy Abou-Hamad[2], Suzana P. Nunes[1†]**



**Development of the new-generation membranes for tunable molecular separation requires materials with abilities beyond strict separation. Stimuli response could remotely adjust the membrane selectivity. Azobenzene derivatives can be photo-switched between trans and cis isomers under ultraviolet or visible light. Here, the azobenzenes were implanted as light switches to bridge the flexible cyclen building blocks. The smart covalent organic network membranes fold and unfold as origami that can be photo-switched between on-state (large) and off-state (small) pores. The cis membranes with off state under ultraviolet (UV) light have higher dye rejection than trans membranes with on-state channels. By controlling the trans-to-cis azobenzene isomerization via UV/Vis light, the pore size can be remotely controlled at the molecular level and the solvent permeance and dye rejection can be dynamically tuned.**

## INTRODUCTION

Smart materials, which can change their structures in response to external stimuli, such as pH, chemicals, electric field, heat, and light, have attracted tremendous attention for wide applications in molecular machines, drug delivery, and smart windows (*1*–*4*). Among the external stimuli, light is highly efficient, noninvasive, and environmentally friendly. Since the first discovery of the cis-form azobenzene under ultraviolet (UV) light (*5*), azobenzene has become one of the most widely investigated light-responsive molecular photoswitches between trans and cis isomers (*6*–*10*). The azobenzene derivatives can be converted from trans to cis form upon exposure to ~365-nm UV light, while the reverse cis-to-trans isomerization is achieved under heat or ~450-nm visible (Vis) light irradiation (*11*, *12*). This photoisomerization process induces a corresponding geometrical change from the planar *trans*-azobenzene (~9 Å) to the nonplanar cis isomer (~6 Å) and can convert the light energy directly into mechanical motions such as bending, oscillating, and twisting, which makes them a promising molecule for building actuators (*13*, *14*). Considering these notable structural and geometrical deformation, azobenzene derivatives are usually used as smart on-off photoswitches on a subnanometer level upon light irradiation or thermal treatment (*10*, *15*).

Covalent organic networks (CONs), representing an interesting class of two-dimensional (2D) or 3D network nanomaterials with well-defined topology, periodic lattice, and tunable pore size, can be ingeniously constructed via strong covalent bonds (*16*–*18*). Compared to the traditional metal-organic frameworks and zeolitic imidazolate frameworks, CONs have the desirable features of low mass density, totally organic metal-free backbone, well-defined topology, permanent porosity, structural diversity, high surface area, and high stability in water (*19*–*21*). The strong covalent bonds render CONs outstanding stability in both aqueous and organic solvents. As a result, CONs have gained noteworthy attention for potential applications in gas adsorption and separation (*22*–*24*), energy storage and conversion (*25*, *26*), optoelectronics (*27*), chemical sensing (*28*), drug delivery (*29*), and catalysis for $CO_2$ reduction or $H_2$ generation (*30*–*32*). Currently, CON and azobenzene derivatives are in the limelight of research for potential applications in optical switching, optical data storage, and photo-robotics. The incorporation of azobenzene groups into CON is a key way to implant smart on-off photoswitches into the network structures, which leaves them with convertible properties in response to external stimuli. Zhang *et al.* (*33*) explored azobenzene units as building blocks to synthesize azo-containing covalent organic frameworks; however, the photoisomerization of azobenzene units in the network skeleton could not be achieved, and the pore size of the network did not really change because of the skeleton rigidity. When the azobenzene units are located in a rigid network skeleton, their motions are restricted and, therefore, the isomerization might be hampered (*34*). Therefore, most other approaches introduce azobenzene units as dangling groups, which have enough free space for isomerization (*35*, *36*). The main problem of this strategy is, again, to provide the freedom and enough free space needed for trans-to-cis azobenzene conversion.

Different from introducing azobenzene as side groups, in this work, the azobenzene is implanted as light-switchable linkers to bridge the flexible building blocks, 1,4,7,10-tetraazacyclododecane (cyclen). Similar to crown ethers, cyclen is a flexible macrocycle (*37*, *38*). There are two types of hydrogens in cyclen: (i) four attached to nitrogen and (ii) eight attached to the carbon atoms. From the viewpoint of stereochemistry, the 12-membered rings would suffer a corresponding chair-to-boat stereoisomerism change in response to the trans-to-cis azobenzene isomerization under UV (*39*–*44*). Here, cyclen has a deformable and flexible ring, while azobenzenes are quite efficient and reliable on-off photoswitches. The resulting smart CON containing the light-switchable azobenzene units and deformable cyclen rings fold and unfold like an origami (Fig. 1) or similar to reversible breathing lungs. The isomerization provides the large geometrical change. The light-responsive pores of self-standing CON membranes can be switched between on and off for precise molecular sieving separations and high solvent permeance.

[1]Biological and Environmental Science and Engineering Division (BESE), Advanced Membranes and Porous Materials Center (AMPM), King Abdullah University of Science and Technology (KAUST), Thuwal 23955-6900, Saudi Arabia. [2]Core Labs, King Abdullah University of Science and Technology, Thuwal 23955, Saudi Arabia.
*Present address: Department of Chemical Engineering, Massachusetts Institute of Technology (MIT), Cambridge, MA 02139, USA.
†Corresponding author. Email: suzana.nunes@kaust.edu.sa

## RESULTS

### Fabrication of the self-standing CON films

Self-standing CON films were developed without any catalyst at the interface between water and mixed hexane/dichloromethane organic phase. Before the best optimized interfacial polymerization (IP) condition (water and hexane/dichloromethane system) was identified, two others were explored: one used water and hexane; the other, water and dichloromethane. In the traditional water and hexane IP system, the monomer cyclen (C) was dissolved in water as the bottom phase and the monomer azobenzene-4,4′-dicarbonyl dichloride (AB) in hexane as the top phase, as indicated in fig. S1. Because AB has limited solubility (0.2 mmol) in hexane, the thickness of the resulting thin film increased only from about 10 to 20 nm by increasing the monomer C concentration from 0.5 to 1.5 mmol. As shown in movie S1, taking such a thin film out from the reaction solution and transferring it onto anodized aluminum oxide (AAO) substrates for

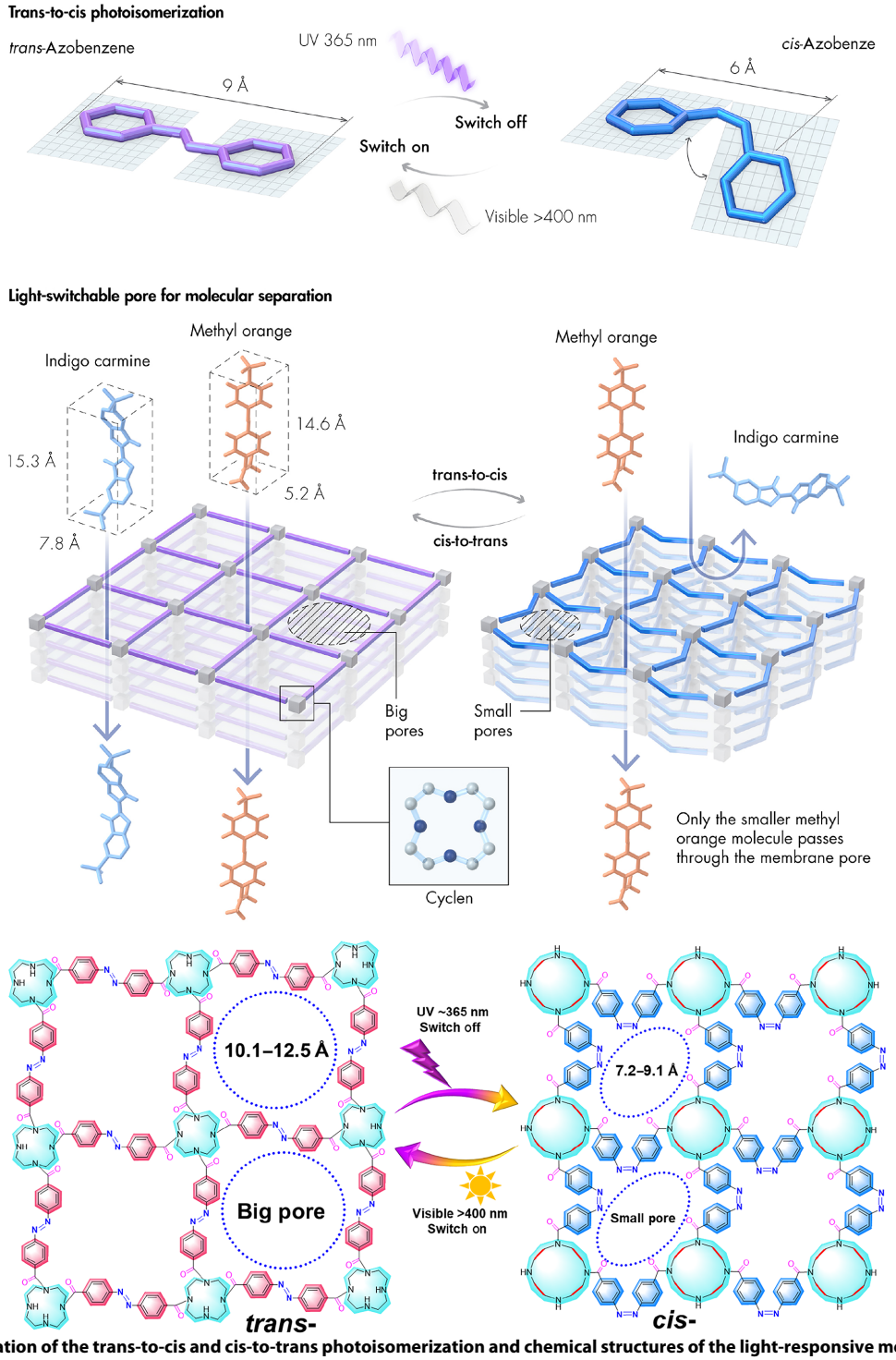


**Fig. 1. Schematic illustration of the trans-to-cis and cis-to-trans photoisomerization and chemical structures of the light-responsive membranes.**

the nanofiltration test is challenging. To fabricate thicker films with sufficient mechanical strength for the nanofiltration test, the surfactant SDS was added to the water phase to improve the IP. Owing to its amphiphilicity, the SDS facilitates the diffusion of monomer C from aqueous to organic phase and extends the interfacial space between the two immiscible phases. The thickness of the resulting films increased, but the films became porous with defects. The membranes in the nanofiltration test had low rejection for dyes.

To fabricate defect-free films with sufficient mechanical strength, the water/dichloromethane system was explored, because the AB monomers have a good solubility in dichloromethane. Therefore, AB was dissolved in dichloromethane as the bottom phase and C was dissolved in water as the top phase, as presented in fig. S2. The resulting membrane had a thickness of about 6 μm and could be easily taken out from the reaction solution and transfer onto AAO substrates for the nanofiltration test, but it is extremely porous, as seen from the cross-sectional scanning electron microscopy (SEM) images, and had defects on both top and bottom surfaces. The catalyst potassium carbonate ($K_2CO_3$) and surfactant SDS were added to enhance the interfacial reaction, but the resulting films became more porous and defective. Comparing the water/dichloromethane system with the water/hexane system, the resulting film thickness mainly depends on the interfacial layer thickness between the two immiscible phases. Here, the interfacial layer of water/dichloromethane was thicker than that of water/hexane, resulting in thicker and more porous films, as shown in movie S2.

On the basis of the previous water/hexane and water/dichloromethane systems, water combined with a mixed hexane/dichloromethane system was then proposed. As shown in fig. S3, AB was dissolved in mixed hexane/dichloromethane (4/1) as the top phase, and C was dissolved in water as the bottom phase. The film thickness increased by increasing the monomer concentration, as presented from the cross-sectional SEM images in fig. S3 (3-1 to 3-4). The membranes became denser and uniform when increasing the interfacial reaction time from 24 to 72 hours, as presented in fig. S3 (3-4 to 3-6). In this IP process, the monomer concentration and mixed solvents were critical for the fabrication of defect-free CON films. The addition of $K_2CO_3$ as catalyst and the surfactant SDS could enhance the interfacial reaction, but the resulting films became more porous and defective, while increasing the monomer concentration and reaction time densified the film layer. Last, the optimized IP condition was found using water and a mixed hexane/dichloromethane system (3-6). AB (153.6 mg, 0.5 mmol) was dissolved in 100 ml of hexane/dichloromethane (4/1) mixture, and C (258.3 mg, 1.5 mmol) was dissolved in 100 ml of water. There was no addition of any surfactant and catalyst because of the self-catalytic nature of cyclen, which could neutralize the hydrochloric acid generated in the interfacial reaction. Because of the self-sealing and self-termination features of the interfacial reaction, the resultant self-standing and defect-free CON films were about 50 nm thick, but they had sufficient mechanical strength and could easily be taken out from water for the nanofiltration tests. As shown in movie S3, no visible tearing or fragmentation occurred after submitting the film to several successive stresses, and this strongly verifies their mechanical robustness. Now, in our laboratory, the continuous crack-free CON thin films can be obtained on a 10-cm scale limited by the dimension of petri dishes, as shown in fig. S3.

### Characterization of trans-to-cis photoisomerization

Figure 1 shows the chemical structures of trans- and cis-CON films. Here, the Fourier transform infrared spectroscopy (FTIR) and x-ray photoelectron spectroscopy (XPS) were applied to characterize chemical structures of the original trans-CON films. As depicted in fig. S4, when comparing the FTIR spectra of both monomers and the trans-CON film, it is found that the imine N—H stretching bands from cyclen at 3250 to 3340 $cm^{-1}$ and the C—Cl stretching bands from AB monomer at about 700 $cm^{-1}$ all disappear, while the strong N═N characteristic peak near 1590 $cm^{-1}$ appears in the resultant trans-CON (AB-C) film, which confirms the successful reaction between AB and C monomers without any catalyst. In addition, the shift of the C═O stretching peak from 1725 to 1715 $cm^{-1}$ indicates the formation of imide linkages between AB and C building blocks. Generally, the disappearance of characteristic N—H and C—Cl groups from the precursor building blocks proves a successful IP reaction. XPS analyses in fig. S4 provide additional evidence for the reaction between AB and C building blocks. The O1s peak at 532 eV can be assigned to the C═O group from AB building blocks, while the C1s spectrum at 285 eV can be attributed to the carbon backbone from AB and C building blocks. At the same time, the N1s spectrum at about 400.3 eV can be attributed to the N═N and C—N groups. To quantitatively calculate these two kinds of nitrogen bonds, the N1s peak was deconvoluted into two peaks at 400.5 eV (N═N from azobenzene units) and 399.8 eV (C—N from cyclen units). The ratio of N═N/C—N from the integrated area is about 1.16, and the estimated azobenzene/cyclen ratio is 2.32, which agrees well with the molecular building ratio (azobenzene/cyclen = 2/1), shown in Fig. 1. The azobenzene/cyclen ratio evaluated from thermogravimetric analysis (TGA) curves is 1.6, as shown in fig. S10. Generally, the calculated atomic composition of C/N/O from XPS spectra is 78.9/11.6/9.5, matching well with their theoretical value of 75.0/16.7/8.3%.

Figure 2 (A to C) shows the photographs of self-standing trans-CON films fabricated via interfacial reaction, supported by the wire loop and AAO substrate. The thickness of this film is about 50 nm, as evaluated from the cross-sectional SEM image of the thin film edge (Fig. 2D). Furthermore, the height analyses measured by atomic force microscopy (AFM) from the silicon wafer to the nanofilm top surface also confirmed the thickness of about 52 nm, as presented in Fig. 2 (G and H). During the interfacial reaction, the region between water and organic interface has a molecule-level thickness; in this confined space, the molecule building blocks were forced to generate a 2D CON layer. Layer-by-layer growth at the interface is the main mechanism to form self-standing CON films with good mechanical robustness.

The bottom and top surface morphologies are different, as presented in Fig. 2 (E and F), mainly in terms of the features sizes. The kind of ridge-and-plain crumpled structure seen on the top is also slightly different from the conventional ridge-and-valley structure of polyamide via IP (*45*) and different from the bottom surface structure. A further close inspection of the AFM image in Fig. 2I also confirms the crumpled top surface morphology. This characteristic crumpled structure may be formed by the cyclen diffusion from aqueous phase to organic phase or the heat dissipation from exothermic cross-linking reaction. Although the exact mechanism leading to the morphology of interfacially polymerized films is complex and still a topic of discussion, there is a consensus that it results from a balance of all interfacial reaction parameters (monomer concentration, reaction time, reaction temperature, and type of solvents). When AB was

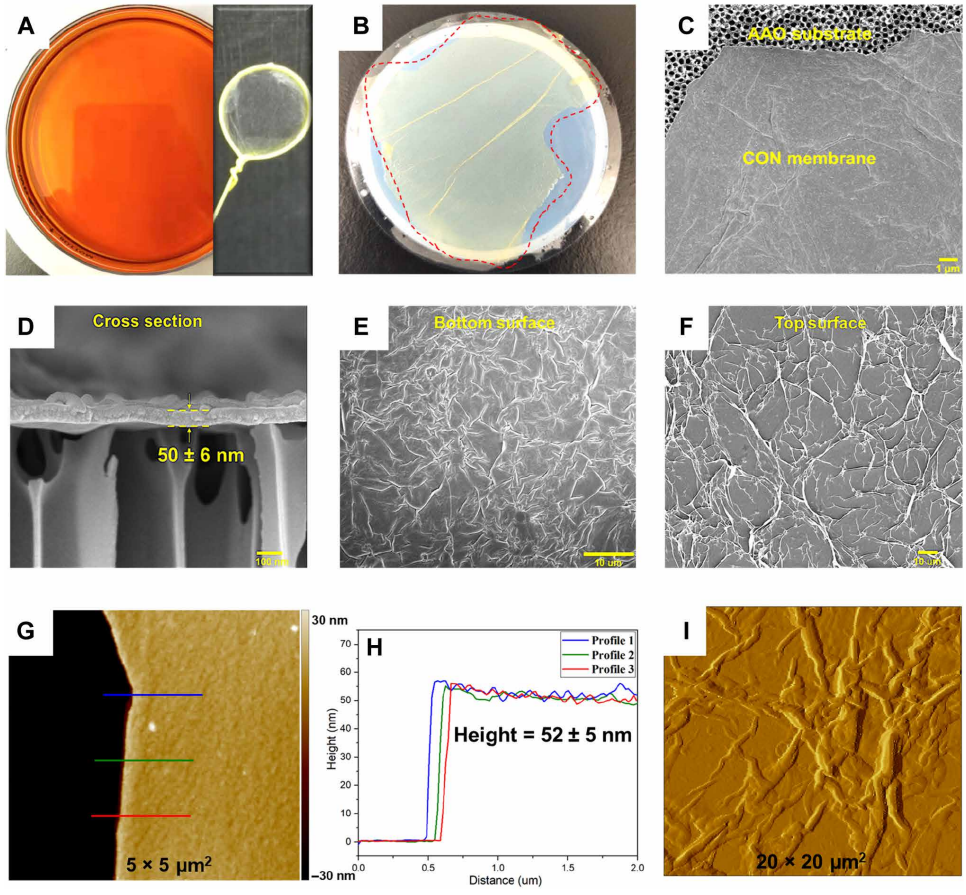


**Fig. 2. Morphology of the freestanding CON membranes.** (**A**) Photographs of the freestanding CON films floating in reaction solvent and supported by a wire loop. (**B**) CON films on AAO substrate. (**C**, **E**, and **F**) Surface and (**D**) cross-sectional SEM images of CON membranes. (**G** to **I**) Thickness and surface morphology evaluated from AFM micrographs. Photo credits: Jiangtao Liu [(A) and (B)].

dissolved in mixed hexane/dichloromethane (3/2) as the top phase and C in water as the bottom phase, as shown in fig. S3 (3-7), the top surface morphology was rougher and more crumpled than the optimal sample (3-6), which was presented in Fig. 2. This ridge-plain-valley structure can increase the membrane surface area, which is helpful for the solvent permeation.

The photoisomerization of the self-standing CON membrane was then analyzed. Both the trans-to-cis isomerization and the cis-to-trans relaxation were performed. The original trans-CON membrane shows a strong absorption maximum peak at 325 nm, arising from the π-π* azobenzene transition. When under UV 365-nm light irradiation, as shown in Fig. 3A, the intensity of the π-π* absorption band at 325 nm decreased rapidly; meanwhile, the weak band at 440 nm corresponding to n-π* transition increased. The trans-to-cis change under UV was extremely fast even with just 1-min irradiation and could reach an almost photostationary state after 5 min. The percentage of the cis-state azobenzene unit in the membrane at 5 min was about 68% (Fig. 3C). This rapid UV light response was similar to the pure AB, as shown in fig. S6. The reversible cis-to-trans process could be fully achieved after 30-min visible light irradiation, as presented in Fig. 3 (B and D); the peak of the π-π* absorption band at 325 nm increased and almost fully recovered; meanwhile, the other peak at 440 nm corresponding to n-π* transition decreased. Repeated UV/Vis irradiation cycles induced the reversible trans-cis-trans changes in the membrane. The ratio of cis or trans state in the membrane could be evaluated from the UV spectra and adjusted by the irradiation time. It should be noted that the cis-to-trans relaxation in the dark needed about 2 days at room temperature.

To help understand the structure differences between trans- and cis-CON membranes, the solid-state nitrogen and proton nuclear magnetic resonance (NMR) of the dry CON membranes were investigated (*46*, *47*). As presented in fig. S7, the $^{15}$N NMR resonance of *trans*-Ph—N═N—Ph is observed at 505 parts per million (ppm), while after UV light irradiation, this peak shifts from 505 to 530 ppm for *cis*-Ph—N═N—Ph, indicating the successful deformation from the trans to cis state. In addition, the characteristic peak at 505 ppm almost disappears in the final cis-CON membranes, which confirms a complete conversion of trans-to-cis photoisomerization under UV 365-nm light. The other two peaks at 175 and 125 ppm are attributed to the nitrogen of C—N and N—H in cyclen units. The $^{1}$H NMR peaks of *trans*-Ph—N═N—Ph (π-π*) shift to right after UV light irradiation, which indicates a weak conjugation of *cis*-Ph—N═N—Ph (n-π*). Note that the single $^{1}$H NMR peak of cyclen unit splits into two peaks from chair-to-boat or chair–to–twisted boat stereoisomerism change.

As revealed from grazing incident diffraction (GID) analysis in fig. S8, the first intense peak at a low 2θ angle of 2.7° shows the ordered stacking of 2D CON layers in membranes. Furthermore, the

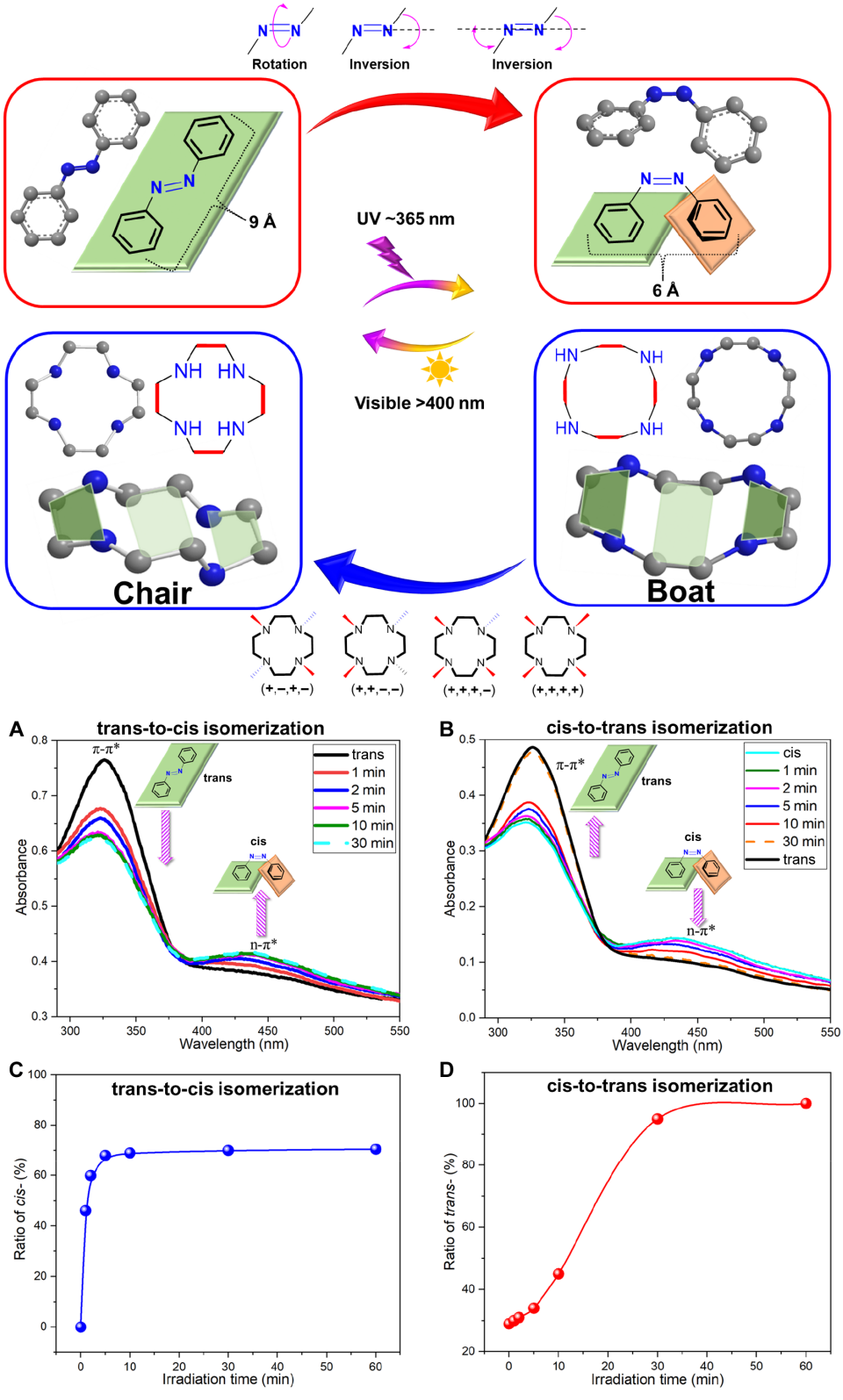


**Fig. 3. The trans-cis-trans reversible isomerization of CON membranes.** (**A**) UV/Vis spectra of trans-to-cis isomerization under UV light and (**B**) cis-to-trans reversible isomerization under visible light. (**C**) Ratio of cis state with UV irradiation time; the membrane is initially in 100% trans state. (**D**) Ratio of trans state with visible light irradiation time; the membrane is initially in 72% cis state.

x-ray diffraction (XRD) was applied to quantify the changes of pore size before and after the UV light irradiation. As shown in fig. S8, the original trans-CON nanofilm has an intense peak at a lower 2θ value of 8.4°, which is assigned to the reflection of CON networks with an open pore aperture of about 10.6 Å. This peak splits into two peaks for cis-CON film; one is still in the position, and the other one shifts to a little higher 2θ value of 11.7°, indicating its slightly smaller pore aperture of 7.5 Å. The pore size shrinks from 10.6 to 7.5 Å in the trans-to-cis isomerization process under UV. Meanwhile, the cyclen units with structural flexibility adjoining azobenzene have chair-to-boat conformation change in response to the trans-to-cis isomerization. The cyclen ring size extends, which is proved by the last broad peak, shifting from a high 2θ angle of 22.8° for the trans-CON nanofilm to a lower 2θ angle of 19.5° for the cis-CON nanofilm. The pore sizes evaluated from XRD results match well with the predicated aperture sizes of trans-CON (10.1 to 12.5 Å) and cis-CON (7.2 to 9.1 Å) films presented in Fig. 1.

## Performance of trans- and cis-CON membranes

Figure 4A shows pure solvent permeance of trans-CON membranes as a function of their inverse viscosity. As the viscosity decreases, the permeance increases following the order of acetonitrile (56.7 liters $m^{-2}$ $hour^{-1}$ $bar^{-1}$) > acetone (48.2 liters $m^{-2}$ $hour^{-1}$ $bar^{-1}$) > methanol (31.6 liters $m^{-2}$ $hour^{-1}$ $bar^{-1}$) > ethanol (12.4 liters $m^{-2}$ $hour^{-1}$ $bar^{-1}$) > isopropanol (6.8 liters $m^{-2}$ $hour^{-1}$ $bar^{-1}$) > dimethylformamide (4.3 liters $m^{-2}$ $hour^{-1}$ $bar^{-1}$). Here, the solvent permeances almost linearly depend on 1/η. Note that the trans-CON film has a pure methanol permeance (31.6 liters $m^{-2}$ $hour^{-1}$ $bar^{-1}$) about 65 times higher than that of the commercially available organic solvent nanofiltration (OSN) membrane DuraMem DM150 (0.48 liters $m^{-2}$ $hour^{-1}$ $bar^{-1}$) (*48*). The preliminary performance results obtained

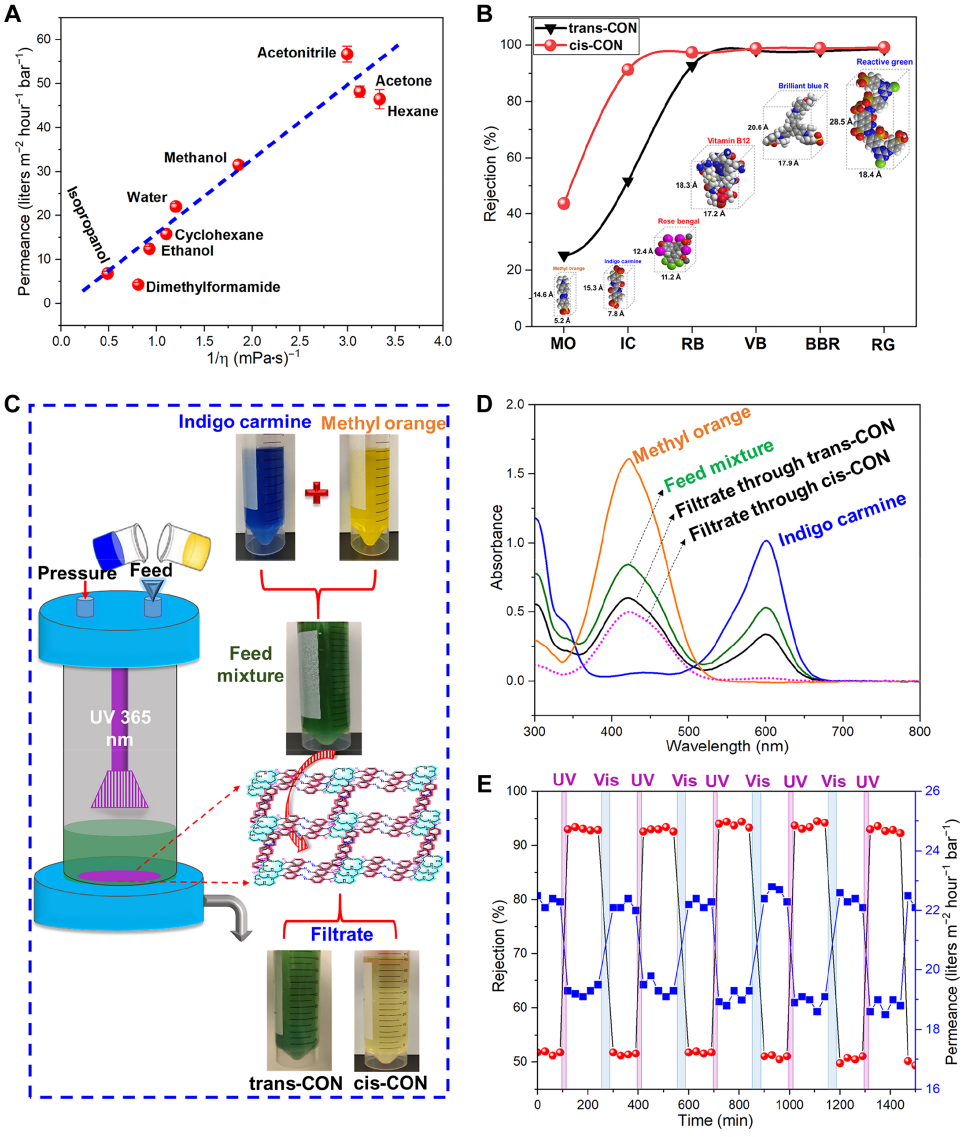


**Fig. 4. Molecular separation performance of the membranes.** (**A**) Permeances of organic solvents through the self-standing trans-CON membranes. (**B**) Rejection ability of trans- and cis-CON membranes toward dyes with different molecular sizes. (**C** and **D**) Separation performance of mixed dyes through trans- and cis-CON membranes. (**E**) IC separation performance in consecutive cycles under UV/Vis light. Photo credits: Jiangtao Liu (C).

with the CON membranes surpass many reported for OSN, as shown in table S1. Therefore, independently of the light response, the high solvent permeances and rejection could be advantageous for the recovery of solvents of pharmaceutical and petrochemical industries with improved energy efficiency. This high permeance can be ascribed to their intrinsic microporosity with regular and semirigid segments forming permanent channels for a rapid solvent transport. In contrast, the conventional polyamide-based membranes are constituted by a randomly formed twisted network, leading to channels of high tortuosity, which increase the solvent transport pathway. Generally, the solvent permeances through CON membranes are governed by network aperture size, solvent viscosity, relative polarity, and solvent-membrane interactions. Usually, the larger the aperture size and the lower the solvent viscosity, the higher is the permeance. The solvent properties including viscosity, relative polarity, kinetic diameter, and total Hansen solubility parameter are summarized in table S2 in the Supplementary Materials. The CON membrane has relatively hydrophilic channels with polar C—N covalent bonds on its pore walls, which have a favorable affinity toward polar solvent molecules. The membrane aperture size and the solvent viscosity are probably the predominant factors, but the relative polarity is also very important. An indication of that is the lower permeance of low-polarity solvents, such as hexane and cyclohexane, being located slightly under the dashed line, while highly polar solvents, such as acetonitrile, methanol, ethanol, and water, have higher permeances well above the dashed line, as illustrated in Fig. 4A. In this regard, the polar channels lever the transport of polar molecules. Dimethylformamide also has a slightly lower permeance than expected for a permeant with similar viscosity, although it is a polar solvent. This might be related to a particularly strong interaction between *N*,*N*′-dimethylformamide and the amine groups of the CON layer, which retard their transport. We then characterized the cis-CON isomeric film in an analogous way. The results are shown in table S3. A similar trend order of solvent transport was observed but with slightly lower permeances because of smaller off-state channels under UV irradiation.

### Light-controlled "on-off-on" switchable pores

There are important challenges for nanofiltration membranes in general. The increasing contamination of organic micropollutants in environmental and biological systems is one of the serious issues faced by humanity. The releasing of organic micropollutants (pesticides, pharmaceuticals, and dyes) to fresh water causes serious health hazards because most of them are mutagenic or carcinogenic in nature (*49*). In addition to the micropollutant removal, nanofiltration membranes with organic solvent stability are extending their applications to solvent and catalyst recovery during organic solvent-based drug synthesis of pharmaceutical compounds/intermediates. Here, dyes with different molecular dimensions were chosen as the models of organic micropollutants and drugs; the chemical structures, molar weights, and dimensional parameters of various dyes are summarized in table S4. The trans-CON membrane with a periodic lattice shows high rejections to dyes with molecular sizes larger than the membrane pore size. As illustrated in fig. S9, long-term permeance tests from 24 to 120 hours were conducted and the dye concentrations before and after filtration through the trans-CON membranes were determined by UV spectra. The high rejection ratio can be clearly seen from the photographs of the feed, filtrate, and retentate dye solutions. As summarized in Fig. 4B, the trans-CON membranes can almost fully reject reactive green (RG, 25.8 × 18.4 Å), brilliant blue R (BBR, 20.6 × 17.9 Å), vitamin B12 (VB, 18.3 × 17.2 Å), and rose bengal (RB, 12.4 × 11.2 Å), but only partially reject indigo carmine (IC, 14.8 × 7.8 Å) and methyl orange (MO, 14.6 × 5.2 Å). When the trans-CON membrane was irradiated with 365-nm light for just 5 min, the IC rejection improved from 50.4 to 91.8%, while the MO rejection improvement was just from 26.1 to 43.5%. This is evidence that the membrane was transformed into the cis-CON form. The transition of the membrane "on-off" switchable pores from the open to the close state could also be confirmed by the XRD analysis. The pore size of the trans-CON membrane in the switch-on state is about 10.6 Å, while the pore size of the cis-CON membrane in the switch-off state is about 7.5 Å. Here, the effective molecular size (5.2 Å) of MO is smaller than the aperture size of the cis-CON membrane. Therefore, MO can pass freely through the membrane but IC cannot. According to the relationship between rejections and molecular dimensions, the estimated cutoff molecular sizes of trans- and cis-CON membranes are 11.2 and 7.8 Å, separately, which are very close to the aperture sizes measured by XRD.

To further investigate the light-controlled on-off-on switchable pores and precise molecular sieving characteristics, the separation of mixed dyes through cis-CON membrane was conducted. Figure S11 shows the permeation cell equipped with a UV lamp; the UV irradiation time can be switched between on and off states. As illustrated in Fig. 4 (C and D), the mixture of IC (blue) and MO (orange) in methanol has a dark green color. The permeate solution still shows dark green color and low rejection when passing through a trans-CON membrane. However, after filtration through a cis-CON membrane under UV irradiation, the permeate solution becomes yellow. The UV absorption spectra confirm that IC is almost completely rejected, while only the smaller MO molecules can pass through the cis-CON membrane. Before the UV 365-nm light irradiation, both MO and IC can almost freely pass through the trans-CON membrane; the molecular transport mechanisms in the light-responsive membranes are illustrated in Fig. 1. The rejection of MO increases from 25.6% (trans-CON) to 41.8% (cis-CON), and the rejection of IC increases from 49.3% (trans-CON) to 94.7% (cis-CON) after the UV irradiation. This great separation improvement from a trans-CON membrane to a cis-CON membrane is due to the pore size change from 10.6 to 7.5 Å. Clearly, under UV 365-nm light irradiation, the pore size switches from on to off state. In the CONs, the cyclen ring is pulled and enforced to extend from a zigzag conformation (movie S4) to a planar conformation (movie S5), with corresponding sizes changing from 3.4 to 4.5 Å, when the azobenzene unit shrinks from 9 to 6 Å, as illustrated in Fig. 3. Generally, three mechanisms can be summarized to explain the isomerization process of azobenzene: (i) rotary motion around the central N═N double bond (rotation mechanism) and (ii) planar variation of one or (iii) both C—N═N—C angles (inversion mechanism) (*43*). Usually, the trans-to-cis process is a combined effect from both inversion and rotation mechanisms. In this process, the flexible cyclen units linked to azobenzene suffer a chair-to-boat distorted conformation change in response to the trans-to-cis azobenzene isomerization (*39*, *40*). Relying on the *N*-azobenzene bond direction relative to the four nitrogen atom plane, pointing up (+) and down (−) in a pattern, four energetically distinct chair (zigzag) and boat (plane) configurations are possibly existing in the membrane, as shown in Fig. 3. Figure 4E presents five consecutive cycles of the CON membrane irradiated alternately by UV/Vis light. The IC rejection improved from about 50% (trans-CON) to

94% (cis-CON) after 5-min UV irradiation; at the same time, the permeance decreased a little from 22 to 19 liters $m^{-2}$ $hour^{-1}$ $bar^{-1}$. The reverse cis-to-trans isomerization could be achieved after irradiation with visible light for 30 min; this means that the cis-CON was switched back to the basic trans state. It was found that the initial permeances and the separation factor were fully recovered in the reversible photo-switching process. In this process, the trans-cis-trans (on-off-on) reversible structure change could be verified by UV spectra in Fig. 3 and XRD spectra in fig. S8.

## DISCUSSION

Different from the traditional membranes with fixed pore dimensions, in this work, the on-off-on light-switchable pores in CON membranes can be remotely controlled via UV light. From the viewpoint of stereochemistry, the cyclen rings suffer a corresponding chair-to-boat stereoisomerism change in response to the trans-to-cis azobenzene isomerization under UV light. The synergistic isomerization induces pore geometrical changes. Clearly, the membranes with on-off-on light-switchable pores have unique merits, such as in situ size tunability, precise molecular sieving, high solvent permeance, good mechanical flexibility, and fabrication simplicity, which may pave the way to remote control of molecule separation, reactant supply, and valuable drug purification from the pharmaceutical industry. For instance, we could imagine using these membranes in systems where A and B small molecules are used to synthesize a larger molecule C. When the synthesis is completed, the "on-switched" membrane could retain C, but A + B and the solvent would permeate through the membrane for recycling. However, when low-quality products are observed or sometimes small-sized by-products are generated, we may apply the same membrane with "off-switching" channels to reject all the solutes and only recycle the solvent. The strategy designed in this work endows traditional membranes with new vitality and opens up new perspectives for separation science and technology. The concept of switching and continuously tuning the membrane selectivity can be extended to other innovative applications, such as sensor, and the controlled (selective) release of encapsulated drugs or fragrances. However, we acknowledge that a lot would have to be done to integrate these membranes or other light-responsive porous systems into a real process. The time response is one of the important factors for the feasibility of any application. Even if we have promising time response compared to previous developments, the applications have to be carefully identified. A proper module design has to be provided to give access to light during operation.

## MATERIALS AND METHODS

### Materials

AB and C were ordered from Tokyo Chemical Industry Ltd. and used directly in the interfacial reaction. The surfactant SDS and catalyst $K_2CO_3$ were ordered from Sigma-Aldrich and used in the IP reaction. The high-performance liquid chromatography–grade methanol, ethanol, isopropanol, and other organic solvents were purchased from VWR Chemicals and used as received. Deionized (DI) water was generated by a Milli-Q ultrapure water system (Millipore, USA). RG [molecular weight (Mw) = 1419, negative charge], VB (Mw = 1355, negative charge), RB (Mw = 1018, negative charge), BBR (Mw = 826, negative charge), IC (Mw = 466, negative charge), and MO (Mw = 327, negative charge) from Sigma-Aldrich were used as the organic micropollutant models at a concentration of 20 ppm in methanol during OSN tests. The AAO disc substrates with a diameter of 47 mm and a pore size of 0.2 μm were obtained from Whatman and used as the supports for the freestanding CON thin films.

### Fabrication of the self-standing CON films

The flexible CON membranes were fabricated via interfacial reaction between AB and C molecular building blocks without any catalysis. The optimal synthesis procedure was carried out as follows: AB (153.6 mg, 0.5 mmol) was dissolved in 100 ml of hexane/dichloromethane (4/1) mixture, and C (258.3 mg, 1.5 mmol) was dissolved in water. As illustrated in fig. S1, the C water solution was first poured into a glass petri dish as aqueous phase, and then AB solution was slowly added onto the top surface as the organic phase, leaving a stable water/organic interface. Afterward, the petri dish was covered to avoid the airflow and kept in a stable condition. A transparent and smooth thin film was observed at the interface between the two immiscible phases. After the interfacial reaction at room temperature for 72 hours, both the aqueous and organic solutions were drained off, leaving the resultant freestanding CON film in the petri dish. Subsequently, this freestanding thin film was rinsed several times by acetone and DI water to wash away the residual monomers and then transferred to an AAO substrate or preserved in DI water for further characterizations.

### Characterizations

The chemical structures of the freestanding CON membranes were analyzed using attenuated total reflectance FTIR (FTIR-iS10) in the wave number range of 500 to 4000 $cm^{-1}$ as an average of 32 scans with 4 $cm^{-1}$ resolution. 1D $^{1}H$ and $^{15}N$ cross-polarization magic-angle spinning (CP-MAS) solid-state NMR spectra were recorded on a Bruker AVANCE III spectrometer operating at 900 MHz, with a conventional double resonance 4-mm CP-MAS probe. Dry nitrogen gas was used for the sample spinning to prevent degradation of the samples. NMR chemical shifts are reported with respect to the external references tetramethylsilane (TMS) and adamantine for $^{1}H$ and $NH_3$ (0 ppm) for $^{15}N$. The spinning frequency was set to 13 kHz. The following sequence was used: 900 pulse on the proton (pulse length 2.4 s), then a cross-polarization step with a contact time of 2 ms, and, last, acquisition of the $^{15}N$ signal under high-power proton decoupling. The delay between the scan was set to 5 s, to allow the complete relaxation of the $^{1}H$ nuclei, and the number of scans was 50,000. An anodization function (exponential) corresponding to a line broadening of 80 Hz was applied before Fourier transformation. The XRD investigation was carried out using a Bruker D8 Advance system with CuKα (λ = 0.154 nm) as the radiation source, operating at 40 keV with a current of 20 mA. The GID measurements were performed on a Bruker D8 Ultra system, and the incident beam is nearly parallel to the thin films. The average *d*-spacing values were calculated on the basis of Bragg's law ($n\lambda = 2d\sin\theta$), where $n$ is an integer (1, 2, 3), λ represents the x-ray wavelength, $d$ represents the intersegmental spacing between two polymer chains, and θ denotes the XRD angle. XPS was performed on an Amicus equipment to measure the elemental composition of the membranes. The thermal stability of monomers and membranes was evaluated by TGA in a TA Instruments TGA-Q50 equipment from 25 to 800°C with a heat ramp of 5°C/min. The study was carried out in inert (N2) and oxidative (air)

atmosphere. The CON-membrane thickness and surface morphology were analyzed by SEM [FEI Magellan eXtreme high resolution (XHR) SEM]. Samples for cross-sectional images were prepared by freeze fracturing the membranes in liquid nitrogen and then coating with a 3-nm thin film of Ir. The surface morphology was measured by AFM on a Bruker Dimension Icon scanning probe microscope.

The UV/Vis spectral changes of CON membranes under 365-nm light irradiation at different time intervals were collected by a UV/Vis spectrometer (UV-2600, Shimadzu). The membranes were suspended in methanol in a quartz cuvette ($l$ = 10 mm). The percentage of trans-to-cis isomer under UV light irradiation was calculated from the following equation

$$\%\text{cis} = \frac{A_{\text{trans}} - A_t}{A_{\text{trans}}} \times 100\% \quad (1)$$

where $A_{\text{trans}}$ is the maximum absorbance of trans-CON at 325 nm and $A_t$ is the absorbance of the CON membrane at 325 nm under UV light irradiation for time $t$.

### Membrane nanofiltration

In terms of permeance and solute rejection, nanofiltration performance of the CON films was measured using a stainless steel dead-end filtration cell at 1 to 5 bar and room temperature. The filtration cell was equipped with a 365-nm UV lamp (fig. S11), which was purchased from Thorlabs and sealed by using epoxy resin in the filtration cell. The diameter of the whole piece of UV light-emitting diode was 2.1 cm; the distance between the UV lamp and the CON film was fixed at 2.0 cm. The corresponding CON membrane was also cut around this size to maximize the exposure of the membrane under UV light. During the experiment, the UV lamp was connected with an electric power source that was maintained at 5 V and 0.8 A, and the light intensity was 0.2 mW/cm$^2$.The membranes were presoaked in the testing solvents for 2 hours before testing. The feed solution with a dye concentration of 20 ppm in methanol was poured into the permeation cell and stirred at a speed of 300 rpm to minimize the concentration polarization. The solvent flux ($F$) and permeance ($P$) were obtained using the following equations:

The pure solvent permeance ($P$) was calculated by the following equation

$$P = \frac{\Delta w}{\rho A \Delta p \Delta t} \quad (2)$$

where $\Delta w$ refers to the permeate weight increase during the filtration time $\Delta t$, $\Delta P$ is the transmembrane pressure (bar), $A$ is the effective membrane area (m$^2$), and ρ is the density of permeate solvent. The units of $P$ are liters m$^{-2}$ hour$^{-1}$ bar$^{-1}$.

The dye rejection ($R$) was calculated by the following equation

$$R = \left(1 - \frac{C_p}{C_f}\right) \times 100\% \quad (3)$$

where $C_p$ and $C_f$ are the concentration of permeate and feed solutions, respectively. The dye concentrations in the feed and permeate solutions were determined by a NanoDrop UV/Vis spectrophotometer. To exclude the effect of solute adsorption, both permeance and rejection were collected when a steady permeate flux was achieved. At least three parallel membrane samples were tested to obtain reliable solvent permeances and solute rejections.

## SUPPLEMENTARY MATERIALS

Supplementary material for this article is available at http://advances.sciencemag.org/cgi/content/full/6/34/eabb3188/DC1

## REFERENCES AND NOTES


1. F. D. Jochum, P. Theato, Temperature-and light-responsive smart polymer materials. *Chem. Soc. Rev.* **42**, 7468–7483 (2013).
2. S. Yagai, A. Kitamura, Recent advances in photoresponsive supramolecular self-assemblies. *Chem. Soc. Rev.* **37**, 1520–1529 (2008).
3. Y. Zhao, T. Ikeda, *Smart Light-Responsive Materials: Azobenzene Containing Polymers and Liquid Crystals* (John Wiley & Sons, 2009).
4. A. H. Gelebart, D. J. Mulder, M. Varga, A. Konya, G. Vantomme, E. W. Meijer, R. L. B. Selinger, D. J. Broer, Making waves in a photoactive polymer film. *Nature* **546**, 632–636 (2017).
5. G. S. Hartley, The *cis*-form of azobenzene. *Nature* **140**, 281 (1937).
6. G. S. Kumar, D. C. Neckers, Photochemistry of azobenzene-containing polymers. *Chem. Rev.* **89**, 1915–1925 (1989).
7. W. R. Browne, B. L. Feringa, Making molecular machines work. *Nat. Nanotechnol.* **1**, 25–35 (2006).
8. S. Li, N. Prasetya, B. P. Ladewig, Investigation of Azo-COP-2 as a photoresponsive low-energy $CO_2$ adsorbent and porous filler in mixed matrix membranes for $CO_2/N_2$ separation. *Ind. Eng. Chem. Res.* **58**, 9959–9969 (2019).
9. Y. Yu, Materials science: A light-fuelled wave machine. *Nature* **546**, 604–607 (2017).
10. T. Muraoka, K. Kinbara, T. Aida, Mechanical twisting of a guest by a photoresponsive host. *Nature* **440**, 512–515 (2006).
11. J. Henzl, M. Mehlhorn, H. Gawronski, K.-H. Rieder, K. Morgenstern, Reversible *cis–trans* isomerization of a single azobenzene molecule. *Angew. Chem. Int. Ed. Engl.* **45**, 603–606 (2006).
12. H. M. D. Bandara, S. C. Burdette, Photoisomerization in different classes of azobenzene. *Chem. Soc. Rev.* **41**, 1809–1825 (2012).
13. J. Park, D. Yuan, K. T. Pham, J.-R. Li, A. Yakovenko, H.-C. Zhou, Reversible alteration of $CO_2$ adsorption upon photochemical or thermal treatment in a metal–organic framework. *J. Am. Chem. Soc.* **134**, 99–102 (2012).
14. N. Liu, Z. Chen, D. R. Dunphy, Y. B. Jiang, R. A. Assink, C. J. Brinker, Photoresponsive nanocomposite formed by self-assembly of an azobenzene-modified silane. *Angew. Chem. Int. Ed.* **42**, 1731–1734 (2003).
15. N. Yanai, T. Uemura, M. Inoue, R. Matsuda, T. Fukushima, M. Tsujimoto, S. Isoda, S. Kitagawa, Guest-to-host transmission of structural changes for stimuli-responsive adsorption property. *J. Am. Chem. Soc.* **134**, 4501–4504 (2012).
16. A. P. Côté, A. I. Benin, N. W. Ockwig, M. O'Keeffe, A. J. Matzger, O. M. Yaghi, Porous, crystalline, covalent organic frameworks. *Science* **310**, 1166–1170 (2005).
17. D. Beaudoin, T. Maris, J. D. Wuest, Constructing monocrystalline covalent organic networks by polymerization. *Nat. Chem.* **5**, 830–834 (2013).
18. X. Feng, X. Ding, D. Jiang, Covalent organic frameworks. *Chem. Soc. Rev.* **41**, 6010–6022 (2012).
19. J. L. Segura, M. J. Mancheño, F. Zamora, Covalent organic frameworks based on Schiff-base chemistry: Synthesis, properties and potential applications. *Chem. Soc. Rev.* **45**, 5635–5671 (2016).
20. S.-Y. Ding, W. Wang, Covalent organic frameworks (COFs): From design to applications. *Chem. Soc. Rev.* **42**, 548–568 (2013).
21. P. Manchanda, S. Chisca, L. Upadhyaya, V.-E. Musteata, M. Carrington, S. P. Nunes, Diffusion-induced in situ growth of covalent organic frameworks for composite membranes. *J. Mater. Chem. A* **7**, 25802–25807 (2019).
22. F. Hiroyasu, O. M. Yaghi, Storage of hydrogen, methane, and carbon dioxide in highly porous covalent organic frameworks for clean energy applications. *J. Am. Chem. Soc.* **131**, 8875–8883 (2009).
23. N. Huang, X. Chen, R. Krishna, D. Jiang, Two-dimensional covalent organic frameworks for carbon dioxide capture through channel-wall functionalization. *Angew. Chem. Int. Ed.* **54**, 2986–2990 (2015).
24. H.-L. Qian, C.-X. Yang, X.-P. Yan, Bottom-up synthesis of chiral covalent organic frameworks and their bound capillaries for chiral separation. *Nat. Commun.* **7**, 12104 (2016).
25. F. Xu, H. Xu, X. Chen, D. Wu, Y. Wu, H. Liu, C. Gu, R. Fu, D. Jiang, Radical covalent organic frameworks: A general strategy to immobilize open-accessible polyradicals for high-performance capacitive energy storage. *Angew. Chem. Int. Ed.* **54**, 6814–6818 (2015).
26. C. R. DeBlase, K. E. Silberstein, T.-T. Truong, H. D. Abruña, W. R. Dichtel, β-Ketoenamine-linked covalent organic frameworks capable of pseudocapacitive energy storage. *J. Am. Chem. Soc.* **135**, 16821–16824 (2013).

27. N. Keller, D. Bessinger, S. Reuter, M. Calik, L. Ascherl, F. C. Hanusch, F. Auras, T. Bein, Oligothiophene-bridged conjugated covalent organic frameworks. *J. Am. Chem. Soc.* **139**, 8194–8199 (2017).
28. S. Dalapati, S. Jin, J. Gao, Y. Xu, A. Nagai, D. Jiang, An azine-linked covalent organic framework. *J. Am. Chem. Soc.* **135**, 17310–17313 (2013).
29. Q. Fang, J. Wang, S. Gu, R. B. Kaspar, Z. Zhuang, J. Zheng, H. Guo, S. Qiu, Y. Yan, 3D porous crystalline polyimide covalent organic frameworks for drug delivery. *J. Am. Chem. Soc.* **137**, 8352–8355 (2015).
30. S. Lin, C. S. Diercks, Y.-B. Zhang, N. Kornienko, E. M. Nichols, Y. Zhao, A. R. Paris, D. Kim, P. Yang, O. M. Yaghi, C. J. Chang, Covalent organic frameworks comprising cobalt porphyrins for catalytic $CO_2$ reduction in water. *Science* **349**, 1208–1213 (2015).
31. V. S. Vyas, F. Haase, L. Stegbauer, G. Savasci, F. Podjaski, C. Ochsenfeld, B. V. Lotsch, A tunable azine covalent organic framework platform for visible light-induced hydrogen generation. *Nat. Commun.* **6**, 8508 (2015).
32. P. Pachfule, A. Acharjya, J. Roeser, T. Langenhahn, M. Schwarze, R. Schomäcker, A. Thomas, J. Schmidt, Diacetylene functionalized covalent organic framework (COF) for photocatalytic hydrogen generation. *J. Am. Chem. Soc.* **140**, 1423–1427 (2018).
33. J. Zhang, L. Wang, N. Li, J. Liu, W. Zhang, Z. Zhang, N. Zhou, X. Zhu, A novel azobenzene covalent organic framework. *CrstEngComm* **16**, 6547–6551 (2014).
34. C. Liu, W. Zhang, Q. Zeng, S. Lei, A photoresponsive surface covalent organic framework: Surface-confined synthesis, isomerization, and controlled guest capture and release. *Chem. A Eur. J.* **22**, 6768–6773 (2016).
35. Z. B. Wang, A. Knebel, S. Grosjean, D. Wagner, S. Bräse, C. Wöll, J. Caro, L. Heinke, Tunable molecular separation by nanoporous membranes. *Nat. Commun.* **7**, 13872 (2016).
36. G. Das, T. Prakasam, M. A. Addicoat, S. K. Sharma, F. Ravaux, R. Mathew, M. Baias, R. Jagannathan, M. A. Olson, A. Trabolsi, Azobenzene-equipped covalent organic framework: Light-operated reservoir. *J. Am. Chem. Soc.* **141**, 19078–19087 (2019).
37. M. Meyer, V. Dahaoui-Gindrey, C. Lecomte, R. Guilard, Conformations and coordination schemes of carboxylate and carbamoyl derivatives of the tetraazamacrocycles cyclen and cyclam, and the relation to their protonation states. *Coord. Chem. Rev.* **178–180**, 1313–1405 (1998).
38. H. Sell, A. Gehl, D. Plaul, F. D. Sönnichsen, C. Schütt, F. Köhler, K. Steinborn, R. Herges, Towards a light driven molecular assembler. *Commun. Chem.* **2**, 62 (2019).
39. S. Shinkai, T. Nakaji, Y. Nishida, T. Ogawa, O. Manabe, Photoresponsive crown ethers. 1. Cis-trans isomerism of azobenzene as a tool to enforce conformational changes of crown ethers and polymers. *J. Am. Chem. Soc.* **102**, 5860–5865 (1980).
40. B. Bosnich, C. K. Poon, M. Tobe, Complexes of cobalt (III) with a cyclic tetradentate secondary amine. *Inorg. Chem.* **4**, 1102–1108 (1965).
41. T. Asano, T. Okada, S. Shinkai, K. Shigematsu, Y. Kusano, O. Manabe, Temperature and pressure dependences of thermal cis-to-trans isomerization of azobenzenes which evidence an inversion mechanism. *J. Am. Chem. Soc.* **103**, 5161–5165 (1981).
42. H. Rau, Further evidence for rotation in the π, π* and inversion in the n, π* photoisomerization of azobenzenes. *J. Photochem.* **26**, 221–225 (1984).
43. H. Rau, E. Lueddecke, On the rotation-inversion controversy on photoisomerization of azobenzenes. Experimental proof of inversion. *J. Am. Chem. Soc.* **104**, 1616–1620 (1982).
44. J. G. Cezar, J. R. M. Carvalho, K. Q. Ferreira, Kinetic and thermodynamic studies of aquation reactions in $[RuL_2(mac)]^{q+}$ complexes: [mac= 1,4,8,11-tetraazacyclotetradecane (cyclam) or 1,4,7,10-tetraazacyclododecane (cyclen); and L= $Cl^-$, $OH^-$, $OH_2$]. *Transition Met. Chem. (London)* **44**, 253–261 (2019).
45. R. J. Petersen, Composite reverse osmosis and nanofiltration membranes. *J. Membr. Sci.* **83**, 81–150 (1993).
46. R. D. Curtis, J. W. Hilborn, G. Wu, M. D. Lumsden, R. E. Wasylishen, J. A. Pincock, A nitrogen-15 NMR study of cis-azobenzene in the solid state. *J. Phys. Chem.* **97**, 1856–1861 (1993).
47. A. Lyčka, Carbon-13 and nitrogen-15 NMR spectra of *cis*-and *trans*-azobenzene, 4-monosubstituted and 4, 4'-disubstituted *trans*-azobenzenes. *Collect. Czech. Chem. Commun.* **47**, 1112–1120 (1982).
48. S. Karan, Z. Jiang, A. G. Livingston, Sub–10 nm polyamide nanofilms with ultrafast solvent transport for molecular separation. *Science* **348**, 1347–1351 (2015).
49. R. P. Schwarzenbach, B. I. Escher, K. Fenner, T. B. Hofstetter, C. A. Johnson, U. von Gunten, B. Wehrli, The challenge of micropollutants in aquatic systems. *Science* **313**, 1072–1077 (2006).
50. M. F. Jimenez-Solomon, Q. Song, K. E. Jelfs, M. Munoz-Ibanez, A. G. Livingston, Polymer nanofilms with enhanced microporosity by interfacial polymerization. *Nat. Mater.* **15**, 760–767 (2016).
51. Y. Feng, M. Weber, C. Maletzko, T.-S. Chung, Facile fabrication of sulfonated polyphenylenesulfone (sPPSU) membranes with high separation performance for organic solvent nanofiltration. *J. Membr. Sci.* **549**, 550–558 (2018).
52. M. H. D. A. Farahani, D. Hua, T.-S. Chung, Cross-linked mixed matrix membranes consisting of carboxyl-functionalized multi-walled carbon nanotubes and P84 polyimide for organic solvent nanofiltration (OSN). *Sep. Purif. Technol.* **186**, 243–254 (2017).
53. A. A. Tashvigh, T.-S. Chung, Facile fabrication of solvent resistant thin film composite membranes by interfacial crosslinking reaction between polyethylenimine and dibromo-p-xylene on polybenzimidazole substrates. *J. Membr. Sci.* **560**, 115–124 (2018).
54. J. Geens, K. Peeters, B. Van der bruggen, C. Vandecasteele, Polymeric nanofiltration of binary water–alcohol mixtures: Influence of feed composition and membrane properties on permeability and rejection. *J. Membr. Sci.* **255**, 255–264 (2005).
55. D. Y. Xing, S. Y. Chan, T.-S. Chung, The ionic liquid [EMIM]OAc as a solvent to fabricate stable polybenzimidazole membranes for organic solvent nanofiltration. *Green Chem.* **16**, 1383–1392 (2014).
56. M. H. D. A. Farahani, D. Hua, T.-S. Chung, Cross-linked mixed matrix membranes (MMMs) consisting of amine-functionalized multi-walled carbon nanotubes and P84 polyimide for organic solvent nanofiltration (OSN) with enhanced flux. *J. Membr. Sci.* **548**, 319–331 (2018).
57. D. Hua, T.-S. Chung, Polyelectrolyte functionalized lamellar graphene oxide membranes on polypropylene support for organic solvent nanofiltration. *Carbon* **122**, 604–613 (2017).
58. S. Hermans, E. Dom, H. Mariën, G. Koeckelberghs, I. F. J. Vankelecom, Efficient synthesis of interfacially polymerized membranes for solvent resistant nanofiltration. *J. Membr. Sci.* **476**, 356–363 (2015).
59. F. Yuan, Y. Yang, R. Wang, D. Chen, Poly(vinylidene fluoride) grafted polystyrene (PVDF-*g*-PS) membrane based on in situ polymerization for solvent resistant nanofiltration. *RSC Adv.* **7**, 33201–33207 (2017).
60. S. Darvishmanesh, J. Degreve, B. Van der Bruggen, Mechanisms of solute rejection in solvent resistant nanofiltration: The effect of solvent on solute rejection. *Phys. Chem. Chem. Phys.* **12**, 13333–13342 (2010).
61. J. Aburabie, K.-V. Peinemann, Crosslinked poly(ether block amide) composite membranes for organic solvent nanofiltration applications. *J. Membr. Sci.* **523**, 264–272 (2017).
62. Y. C. Xu, Y. P. Tang, L. F. Liu, Z. H. Guo, L. Shao, Nanocomposite organic solvent nanofiltration membranes by a highly-efficient mussel-inspired co-deposition strategy. *J. Membr. Sci.* **526**, 32–42 (2017).
63. H. Mariën, I. F. J. Vankelecom, Transformation of cross-linked polyimide UF membranes into highly permeable SRNF membranes via solvent annealing. *J. Membr. Sci.* **541**, 205–213 (2017).
64. Y. Xu, F. You, H. Sun, L. Shao, Realizing mussel-inspired polydopamine selective layer with strong solvent resistance in nanofiltration toward sustainable reclamation. *ACS Sustain. Chem. Eng.* **5**, 5520–5528 (2017).
65. H. Fan, J. Gu, H. Meng, A. Knebel, J. Caro, High-flux membranes based on the covalent organic framework COF-LZU1 for selective dye separation by nanofiltration. *Angew. Chem. Int. Ed.* **57**, 4083–4087 (2018).
66. C. Li, S. Li, L. Tian, J. Zhang, B. Su, M. Z. Hu, Covalent organic frameworks (COFs)-incorporated thin film nanocomposite (TFN) membranes for high-flux organic solvent nanofiltration (OSN). *J. Membr. Sci.* **572**, 520–531 (2019).
67. F. Pan, W. Guo, Y. Su, N. A. Khan, H. Yang, Z. Jiang, Direct growth of covalent organic framework nanofiltration membranes on modified porous substrates for dyes separation. *Sep. Purif. Technol.* **215**, 582–589 (2019).
68. R. Wang, X. Shi, A. Xiao, W. Zhou, Y. Wang, Interfacial polymerization of covalent organic frameworks (COFs) on polymeric substrates for molecular separations. *J. Membr. Sci.* **566**, 197–204 (2018).
69. R. Wang, X. Shi, Z. Zhang, A. Xiao, S.-P. Sun, Z. Cui, Y. Wang, Unidirectional diffusion synthesis of covalent organic frameworks (COFs) on polymeric substrates for dye separation. *J. Membr. Sci.* **586**, 274–280 (2019).
70. T. Wang, H. Wu, S. Zhao, W. Zhang, M. Tahir, Z. Wang, J. Wang, Interfacial polymerized and pore-variable covalent organic framework composite membrane for dye separation. *Chem. Eng. J.* **384**, 123347 (2020).
71. A. Buekenhoudt, F. Bisignano, G. De Luca, P. Vandezande, M. Wouters, K. Verhulst, Unravelling the solvent flux behaviour of ceramic nanofiltration and ultrafiltration membranes. *J. Membr. Sci.* **439**, 36–47 (2013).
72. Q. Yang, Y. Su, C. Chi, C. T. Cherian, K. Huang, V. G. Kravets, F. C. Wang, J. C. Zhang, A. Pratt, A. N. Grigorenko, F. Guinea, A. K. Geim, R. R. Nair, Ultrathin graphene-based membrane with precise molecular sieving and ultrafast solvent permeation. *Nat. Mater.* **16**, 1198–1202 (2017).
73. I. M. Smallwood, *Handbook of Organic Solvent Properties* (Butterworth-Heinemann, 2012).


**Acknowledgments:** We thank L. Upadhyaya, D. Mahalingam, and B. Pulido for valuable assistance and fruitful discussion in the research process. The schematic illustration in Fig. 1 was produced by X. Pita, scientific illustrator at King Abdullah University of Science

and Technology (KAUST). **Funding:** We thank King Abdullah University of Science and Technology for the financial support, particularly CRG grant URF/1/3441-01-01. **Author contributions:** J.L. performed the experiments. J.L. and S.P.N. wrote the manuscript. All authors discussed the results and commented on the manuscript. **Competing interests:** The authors declare that they have no competing interests. **Data and materials availability:** The data that support the findings of this study are available within the paper, in the Supplementary Materials, in the KAUST repository, or from the corresponding author on reasonable request.

Submitted 15 February 2020
Accepted 9 July 2020
Published 19 August 2020
10.1126/sciadv.abb3188

**Citation:** J. Liu, S. Wang, T. Huang, P. Manchanda, E. Abou-Hamad, S. P. Nunes, Smart covalent organic networks (CONs) with "on-off-on" light-switchable pores for molecular separation. *Sci. Adv.* **6**, eabb3188 (2020).